ZR Zoological Research

Supplementary Materials

Genome of striped eel catfish (*Plotosus lineatus*) provides insights into the adaptive evolution of amphidromous fish

Feng Shao [1], Ze-Chen Wu [1], Yuan Xu [1], Ping Li [2], Zuo-Gang Peng [1,3,*]

[1] Key Laboratory of Freshwater Fish Reproduction and Development (Ministry of Education), Southwest University School of Life Sciences, Chongqing 400715, China
[2] College of Fisheries, Southwest University, Rongchang, Chongqing 402460, China
[3] Academy of Plateau Science and Sustainability, Qinghai Normal University, Xining, Qinghai 810008, China

*Corresponding author, E-mail: pzg@swu.edu.cn

SUPPLEMENTARY MATERIALS AND METHODS

Sample collection and sequencing

Samples for genome sequencing were collected from female *Plotosus lineatus* from Beibu Gulf, Qin Zhou, Guangxi Province, China (21°44′19.79″ N, 108°34′41.97″ E). The study of *P. lineatus* has been approved by Southwest University IACUC (Institutional Animal Care and Use Committee), IACUC NO. Approved: 20200715-01. Blood, brain, dendritic organ (DO), fins, gills, gonads, gut, heart, head kidney, liver, muscle, skin, and spleen were collected and immediately frozen in liquid nitrogen.

Blood samples were collected for genome sequencing, and DNA was prepared using a QIAGEN® Genomic Kit (Cat No. ID:13343, QIAGEN, Hilden, Germany). *De novo* genome sequencing was performing using high-throughput sequencing, Nanopore PromethION, PacBio Sequel II (circular consensus sequence, CCS), and Hi-C technologies. For MGISEQ 2000 sequencing, we constructed one paired-end library with insert sizes of 200–400 bp, followed by filtering using fastp (Chen et al., 2018) to generate 61.75 Gb of clean data for genome survey and correction. For Nanopore PromethION sequencing, we constructed two long-read libraries. Raw reads in fastq format with a mean_qscore_template<7 were then filtered to generate 115.93 Gb of clean data. For PacBio Sequel II sequencing, we constructed one long-read library (10–20 kb). Raw data were analyzed using Smrtlink software (https://www.pacb.com/support/software-downloads/) to generated 10.28 Gb of clean data. We constructed three Hi-C libraries for Hi-C sequencing and generated clean data at a depth of 122.14 Gb (filtered using fastp).

RNA analysis involved 13 tissues (brain, DO, fin, gill, gonad, gut, heart, head kidney, kidney, liver, muscle, skin, and spleen) extracted using an RNeasy Plus Mini Kit (QIAGEN, Hilden, Germany). Illumina paired-end sequencing (validated RNA samples, Illumina HiSeq4000, 150 bp) was used to prepare a cDNA library with a TruSeq Sample Preparation Kit (Illumina, San Diego, USA). Qualified RNA from 10 tissues (blood, brain, fin, gill, gonad, heart, head kidney, liver, muscle, and spleen) was mixed in equal amounts and reverse transcribed using SQK-PCS109 for ONT (Oxford Nanopore Technologies) library preparation and sequencing (Nanopore PromethION). Raw data were filtered in the same manner as for DNA.

Genome assembly and evaluation

Quality-filtered reads were subjected to 35 mer frequency distribution analysis using Jellyfish (Marçais & Kingsford, 2011). We analyzed the 35 mer depth distribution of clean sequencing reads using FindGSE (Sun et al., 2018) and KMC (Kokot et al., 2017) to estimate *P. lineatus* genome size and heterozygosity (Supplementary Figure S8). Long-read (ONT) assembly was performed using NextDenovo (reads_cutoff: 1 k, seed_cutoff: 32 k, https://github.com/Nextomics/NextDenovo). To improve assembly accuracy, the contigs were refined using default parameters in NextPolish (https://github.com/Nextomics/NextPolish) for long and short reads. To anchor the hybrid scaffolds to the chromosome, they were further clustered, ordered, and oriented on chromosomes using LACHESIS (Korbel & Lee, 2013) with the parameters CLUSTER_MIN_RE_SITES=100, CLUSTER_MAX_LINK_DENSITY=2.5, NONINFORMATIVE RATIO=1.4, ORDER MIN N RES IN TRUNK=60, and ORDER MIN N RES IN SHREDS=60. Finally, the interactive heatmap of the initial assembly results of LACHESIS was drawn according to the interactions between different scaffolds. The position and direction of scaffolds that obviously did not meet the chromosome interaction characteristics in the figure were adjusted. Of note, if a scaffold itself did not meet chromosome interaction characteristics, the scaffold was interrupted. The scaffolds were then adjusted separately until the overall heatmap conformed to the characteristics of chromosome interaction.

To evaluate *P. lineatus* genome assembly quality, we identified single-copy orthologs and conserved eukaryotic core genes in metazoa_odb10 based on the BUSCO database and filtered RNA sequencing (RNA-seq) short reads aligned to the reference genome using hisat2 (Kim et al., 2015) with default parameters (Supplementary Table S22).

Genome annotation

We annotated tandem repeats using GMATA (Wang & Wang, 2016) and TRF (Benson, 1999). For transposable element (TE) annotation, an *ab initio* repeat library for *P. lineatus* was initially

predicted using MITE-hunter (Han & Wessler, 2010) and RepeatModeler2 (Flynn et al., 2020) with default parameters, followed by LTR_FINDER (Xu & Wang, 2007), LTRharverst (Ellinghaus et al., 2008), and LTR_retriver (Ou & Jiang, 2018). RepeatMasker (http://www.repeatmasker.org/) was used to search for known and novel TEs by mapping sequences against the *de novo* repeat and RepBase TE libraries.

RNA-seq-based gene prediction was based on the RNA-seq short-read mapping results (described above). Transcripts were assembled using StringTie (Pertea et al., 2015). Full-length reads were identified and oriented from the sequencing reads using the Pychopper tool (https://github.com/nanoporetech/pychopper) with default parameters. Full-length reads were aligned to the *P. lineatus* reference genome using minimap2 (Li, 2018) with "-ax splice-uf". The aligned full-length reads were clustered using pinfish software (https://github.com/nanoporetech/pinfish) following the official recommendations of Nanopore. Redundancy was removed using cDNA_Cupcake software (https://github.com/Magdoll/cDNA_Cupcake) and polished using a reference genome sequence. The assembled transcripts based on full-length and short reads were merged with open reading frames (ORFs) and predicted using PASA (Haas et al., 2008). For *de novo* prediction, RNA-seq reads were assembled using StringTie (Pertea et al., 2015) and analyzed with PASA (Haas et al., 2008) to produce a training set. AUGUSTUS (Stanke et al., 2008) with default parameters was used for *ab initio* gene prediction using the training set. Homologous proteins of other species (*Bagarius yarrelli*, *Danio rerio*, *Glyptosternon maculatum*, *Hemibagrus* wyckioides, *Homo sapiens*, *Ictalurus punctatus*, *Oryzias latipes*, *Tachysurus fulvidraco*, and *Takifugu rubripes*) were also used to predict protein-coding genes using GeMoMa (Keilwagen et al., 2016). A protein-coding gene dataset was then generated by integrating the three results using EvidenceModeler (Haas et al., 2008). Furthermore, TransposonPSI (http://transposonpsi.sourceforge.net) was used to remove genes containing TEs. To evaluate *P. lineatus* genome annotation quality, we identified single-copy orthologs and conserved eukaryotic core genes in actinopterygii_odb9 based on the BUSCO database. To annotate gene function, the predicted gene sequences were searched against five databases: i.e., SwissProt (Uniprot Consortium, 2021), NR (https://www.ncbi.nlm.nih.gov/refseq/about/nonredundantproteins/), KEGG (Kanehisa & Goto, 2000), KOG (Tatusov et al., 2003), and GO (Gene Ontology Consortium, 2017).

Reconstruction of ancestral karyotype and fusion site analysis

We performed whole-genome alignments across all chromosome-level catfish genomes (*Cranoglanis bouderius*, *H. wyckioides*, *I. punctatus*, *Leiocassis longirostris*, *P. lineatus*, *Silurus meridionalis*, and *T. fulvidraco*) and an outgroup species (*Electrophorus electricus*). First, pairwise whole-genome alignments were obtained between *P. lineatus* and the other species using LASTZ (Harris, 2007) with parameters 'H=2 000, Y=3 400, L=6 000, K=2 200'. Chain/Net was performed using lavToPsl, axtChain, chainPreNet, and chainNet (Kuhn et al., 2013). We then applied the DESCHRAMBLER algorithm (https://github.com/jkimlab/DESCHRAMBLER), chains, and nets generated by LASTZ to generate conserved syntenic fragments across the eight species. Syntenic fragments ≥500 kb in length were used to construct conserved syntenic fragments. Finally, the ancestral genome structures were constructed using ANGES (Jones et al., 2012), and the results less than 1M were filtered out. The final results were drawn in SVG. Rearrangement events in each lineage were inferred using GRIMM (Tesler, 2002). Ancestral chromosome blocks on chromosomes of different species are shown in different colors. Adjacent blocks of different ancestors on the same chromosome are mainly caused by fusion and translocation. In this study, the distance between adjacent color blocks of less than 1 Mb was defined as a fusion and translocation site (FTS). For these FTSs in *P. lineatus*, 500 kb was taken from the center of the two-color blocks upstream and downstream for a total of 1 Mb for subsequent analysis. Combined with the transposon annotation results, we calculated the transposon content in FTSs and other regions of the chromosome (100 kb window), performed rank sum Mann-Whitney tests on FTSs and non-fusion sites, and performed statistical analysis of transposon types in FTSs.

Comparative genomic analysis

We used the MUMmer (Marçais et al., 2018) tool nucmer to perform pairwise whole-genome alignment with the parameter "-b 400." The alignments were filtered to retain the one-to-one best

hits using delta-filt from the MUMmer package. Unanchored scaffolds were excluded from the alignments. The alignments were formatted using the MCscan pipeline (https://github.com/tanghaibao/jcvi) for synteny visualization.

We identified homologous relationships between *P. lineatus* and other species (*Astyanax mexicanus*, *C. bouderius*, *D. rerio*, *E. electricus*, *G. maculatum*, *H. wyckioides*, *L. oculatus*, *O. latipes*, and *S. meridionalis*) by downloading their protein sequences and aligning them using OrthoMCL (Li et al., 2003). Molecular phylogenetic analysis was performed using shared single-copy genes based on orthologous gene sets identified with OrthoMCL. Each ortholog group was aligned multiple times using MAFFT (Kasahara et al., 2007). Poorly aligned sequences were then eliminated using Gblocks (http://molevol.cmima.csic.es/castresana/Gblocks.html), and the GTRGAMMA substitution model in RAxML (Stamatakis, 2014) was used for phylogenetic tree construction with 1 000 bootstrap replicates. Three fossil calibration times were obtained from TimeTree (Kumar et al., 2022). The control time with divergence time parameters was "((*O. latipes*, (*D. rerio*, ((*E. electricus*, (*P. lineatus*, (((*H. wyckioides*, *G. maculatum*), *C. bouderius*), *S. meridionalis*))), *A. mexicanus*)) 'B (126 179)') 'B (205 255)', *L. oculatus*) 'B (291 338)'". To detect the potential genetic basis of the unique characteristics of *P. lineatus*, we performed positive selection analysis based on phylogenetic trees using the branch-site model implemented in PAML (Yang, 1997). A likelihood ratio test (LRT) was conducted to compare models that allowed sites to be under positive selection for *P. lineatus*. *P*-values were computed based on chi-square statistics, and genes with $P<0.05$ were treated as candidate positively selected genes (PSGs). According to the OrthoMCL results, gene family expansions and contractions were detected using CAFE (De Bie et al., 2006) and enrichment tests were performed using ClusterProfiler (Yu et al., 2012), with the same tools used for other enrichment analyses.

For phylogenetic tree reconstruction of the *sox* gene family, we aligned all protein sequences (MUSCLE) and constructed a maximum-likelihood tree using MEGA 11 (Tamura et al., 2021).

Analysis of DO-specific expressed gene

Based on the gene structure results and 13 tissue RNA-seq short-read mapping results, StringTie was used to calculate the expression value of each gene. The expression value in each tissue was then used to calculate the tissue specificity index (TAU) (Yanai et al., 2005) for each gene. Tissue-specific expression was defined as a gene that showed at least two-fold higher expression than in any other tissue, with the highest RPKM (Reads Per Kilobase per Million mapped reads) >1 and TAU>0.8.

To determine whether transposons participate in DO development, RNA-seq data and transposon annotation results of the 13 tissues were used to predict activated transposons using TE candidates (Ohtani et al., 2013) with very demanding parameters (-c=0.9 -l=300). We screened for transposons inserted into genes specifically expressed and activated by the DO.

Identification of venom-related genes and molecular evolution

To study venom-related genes in *P. lineatus*, we used research methods applied for snake venom (Li et al., 2021). We first combined two venom-related protein databases: i.e., manually reviewed sequences from the animal toxin annotation project115 (http://www.uniprot.org/program/Toxins), which systematically annotated venom proteins and toxins from all venomous species, and venom-related proteins reported in a previous article (Xie et al., 2016), which were annotated using Swiss-Prot (Boeckmann et al., 2003). All predicted protein sequences of *P. lineatus* were queried against the combined dataset using BLASTP (Camacho et al., 2009), with a similarity cut-off E-value of 1e-5. Redundant alignments were removed. For each candidate venom-related protein identified, a venom-related gene was manually curated according to the annotations of the closest homologous protein hit in Swiss-Prot. The Swiss-Prot annotation results of the query and target sequences were similar. For comparison, the same analysis was performed for *Ameiurus melas*.

To assess the diversification rates of major venom-related genes in *P. lineatus* and *A. melas*, we first ran all-vs-all BLASTN (E-value≤1e-5) in two species pairs using coding sequences (CDSs) to obtain gene pairs with the highest similarity. Kalign (Lassmann, 2020) was then used to perform pairwise alignment of the gene pairs and output AXT files, which were imported into KaKs_Calculator (Wang et al., 2010). We computed nonsynonymous and synonymous substitution

rates (Ka and Ks) for protein-coding regions of each gene pair using previously reported methods (Yang & Nielsen, 2000). Modified YN (Zhang et al., 2006) and Nei-Gojobori (Nei & Gojobori, 1986) models were also applied simultaneously when invalid Ka/Ks values were generated. Significant differences between venom-like and non-venom gene families were assessed using the Mann-Whitney test.

The genes we focused on (*sox* gene family and *stonustoxin* gene) were based on the manual inspection results according to the collinearity between genes. Briefly, we used Fgenesh+ to re-predict collinear position (region between two gene flanks) of these genes.

References

Benson G. 1999. Tandem repeats finder: a program to analyze DNA sequences. *Nucleic Acids Research*, **27**(2): 573–580.

Boeckmann B, Bairoch A, Apweiler R, et al. 2003. The SWISS-PROT protein knowledgebase and its supplement TrEMBL in 2003. *Nucleic Acids Research*, **31**(1): 365–370.

Camacho C, Coulouris G, Avagyan V, et al. 2009. BLAST+: architecture and applications. *BMC Bioinformatics*, **10**: 421.

Chen SF, Zhou YQ, Chen YR, et al. 2018. fastp: an ultra-fast all-in-one FASTQ preprocessor. *Bioinformatics*, **34**(17): i884–i890.

De Bie T, Cristianini N, Demuth JP, et al. 2006. CAFE: a computational tool for the study of gene family evolution. *Bioinformatics*, **22**(10): 1269–1271.

Ellinghaus D, Kurtz S, Willhoeft U. 2008. *LTRharvest*, an efficient and flexible software for *de novo* detection of LTR retrotransposons. *BMC Bioinformatics*, **9**: 18.

Flynn JM, Hubley R, Goubert C, et al. 2020. RepeatModeler2 for automated genomic discovery of transposable element families. *Proceedings of the National Academy of Sciences of the United States of America*, **117**(17): 9451–9457.

Haas BJ, Salzberg SL, Zhu W, et al. 2008. Automated eukaryotic gene structure annotation using EVidenceModeler and the Program to Assemble Spliced Alignments. *Genome Biology*, **9**(1): R7.

Han YJ, Wessler SR. 2010. MITE-Hunter: a program for discovering miniature inverted-repeat transposable elements from genomic sequences. *Nucleic Acids Research*, **38**(22): e199.

Harris RS. 2007. Improved Pairwise Alignment of Genomic DNA. Ph.D. dissertation, The Pennsylvania State University, State College.

Jones BR, Rajaraman A, Tannier E, et al. 2012. ANGES: reconstructing ANcestral GEnomeS maps. *Bioinformatics*, **28**(18): 2388–2390.

Kanehisa M, Goto S. 2000. KEGG: kyoto encyclopedia of genes and genomes. *Nucleic Acids Research*, **28**(1): 27–30.

Kasahara M, Naruse K, Sasaki S, et al. 2007. The medaka draft genome and insights into vertebrate genome evolution. Nature, **447**(7145): 714–719.

Keilwagen J, Wenk M, Erickson JL, et al. 2016. Using intron position conservation for homology-based gene prediction. *Nucleic Acids Research*, **44**(9): e89.

Kim D, Langmead B, Salzberg SL. 2015. HISAT: a fast spliced aligner with low memory requirements. *Nature Methods*, **12**(4): 357–360.

Kokot M, Długosz M, Deorowicz S. 2017. KMC 3: counting and manipulating *k*-mer statistics. *Bioinformatics*, **33**(17): 2759–2761.

Korbel JO, Lee C. 2013. Genome assembly and haplotyping with Hi-C. *Nature Biotechnology*, **31**(12): 1099–1101.

Kuhn RM, Haussler D, Kent WJ. 2013. The UCSC genome browser and associated tools. *Briefings in Bioinformatics*, **14**(2): 144–161.

Kumar S, Suleski M, Craig JM, et al. 2022. TimeTree 5: an expanded resource for species divergence times. *Molecular Biology and Evolution*, **39**(8): msac174.

Lassmann T. 2020. Kalign 3: multiple sequence alignment of large datasets. *Bioinformatics*, **36**(6): 1928–1929.

Li A, Wang JJ, Sun K, et al. 2021. Two reference-quality sea snake genomes reveal their divergent evolution of adaptive traits and venom systems. *Molecular Biology and Evolution*, **38**(11): 4867–4883.

Li H. 2018. Minimap2: pairwise alignment for nucleotide sequences. *Bioinformatics*, **34**(18): 3094–3100.

Li L, Stoeckert CJ Jr, Roos DS. 2003. OrthoMCL: identification of ortholog groups for eukaryotic genomes. *Genome Research*, **13**(9): 2178–2189.

Marçais G, Delcher AL, Phillippy AM, et al. 2018. MUMmer4: a fast and versatile genome alignment system. *PLoS Computational Biology*, **14**(1): e1005944.

Marçais G, Kingsford C. 2011. A fast, lock-free approach for efficient parallel counting of occurrences of *k*-mers. *Bioinformatics*, **27**(6): 764–770.

Nei M, Gojobori T. 1986. Simple methods for estimating the numbers of synonymous and nonsynonymous nucleotide substitutions. *Molecular Biology and Evolution*, **3**(5): 418–426.

Ohtani H, Iwasaki YW, Shibuya A, et al. 2013. DmGTSF1 is necessary for Piwi-piRISC-mediated transcriptional transposon silencing in the *Drosophila* ovary. *Genes & Development*, **27**(15): 1656–1661.

Ou SJ, Jiang N. 2018. LTR_retriever: a highly accurate and sensitive program for identification of long terminal repeat retrotransposons. *Plant Physiology*, **176**(2): 1410–1422.

Pertea M, Pertea GM, Antonescu CM, et al. 2015. StringTie enables improved reconstruction of a transcriptome from RNA-seq reads. *Nature Biotechnology*, **33**(3): 290–295.

Stamatakis A. 2014. RAxML version 8: a tool for phylogenetic analysis and post-analysis of large phylogenies. *Bioinformatics*, **30**(9): 1312–1313.

Stanke M, Diekhans M, Baertsch R, et al. 2008. Using native and syntenically mapped cDNA alignments to improve *de novo* gene finding. *Bioinformatics*, **24**(5): 637–644.

Sun HQ, Ding J, Piednoël M, et al. 2018. *findGSE*: estimating genome size variation within human and *Arabidopsis* using *k*-mer frequencies. *Bioinformatics*, **34**(4): 550–557.

Tamura K, Stecher G, Kumar S. 2021. MEGA11: molecular evolutionary genetics analysis version 11. *Molecular Biology and Evolution*, **38**(7): 3022–3027.

Tatusov RL, Fedorova ND, Jackson JD, et al. 2003. The COG database: an updated version includes eukaryotes. *BMC Bioinformatics*, **4**: 41.

Tesler G. 2002. GRIMM: genome rearrangements web server. *Bioinformatics*, **18**(3): 492–493.

The Gene Ontology Consortium. 2017. Expansion of the Gene Ontology knowledgebase and resources. *Nucleic Acids Research*, **45**(D1): D331–D338.

The Uniprot Consortium. 2021. UniProt: the universal protein knowledgebase in 2021. *Nucleic Acids Research*, **49**(D1): D480–D489.

Wang DP, Zhang YB, Zhang Z, et al. 2010. KaKs_Calculator 2.0: a toolkit incorporating gamma-series methods and sliding window strategies. *Genomics Proteomics Bioinformatics*, **8**(1): 77–80.

Wang XW, Wang L. 2016. GMATA: an integrated software package for genome-scale SSR mining, marker development and viewing. *Frontiers in Plant Science*, **7**: 1350.

Xie B, Li XF, Lin ZL, et al. 2016. Prediction of toxin genes from Chinese yellow catfish based on transcriptomic and proteomic sequencing. *International Journal of Molecular Sciences*, **17**(4): 556.

Xu Z, Wang H. 2007. LTR_FINDER: an efficient tool for the prediction of full-length LTR retrotransposons. *Nucleic Acids Research*, **35**(S2): W265–W268.

Yanai I, Benjamin H, Shmoish M, et al. 2005. Genome-wide midrange transcription profiles reveal expression level relationships in human tissue specification. *Bioinformatics*, **21**(5): 650–659.

Yang Z. 1997. PAML: a program package for phylogenetic analysis by maximum likelihood. *Computer Applications in the Biosciences*, **13**(5): 555–556.

Yang Z, Nielsen R. 2000. Estimating synonymous and nonsynonymous substitution rates under realistic evolutionary models. *Molecular Biology and Evolution*, **17**(1): 32–43.

Yu GC, Wang LG, Han YY, et al. 2012. ClusterProfiler: an R package for comparing biological themes among gene clusters. *Omics*, **16**(5): 284–287.

Zhang Z, Li J, Yu J. 2006. Computing Ka and Ks with a consideration of unequal transitional substitutions. *BMC Evolutionary Biology*, **6**: 44.

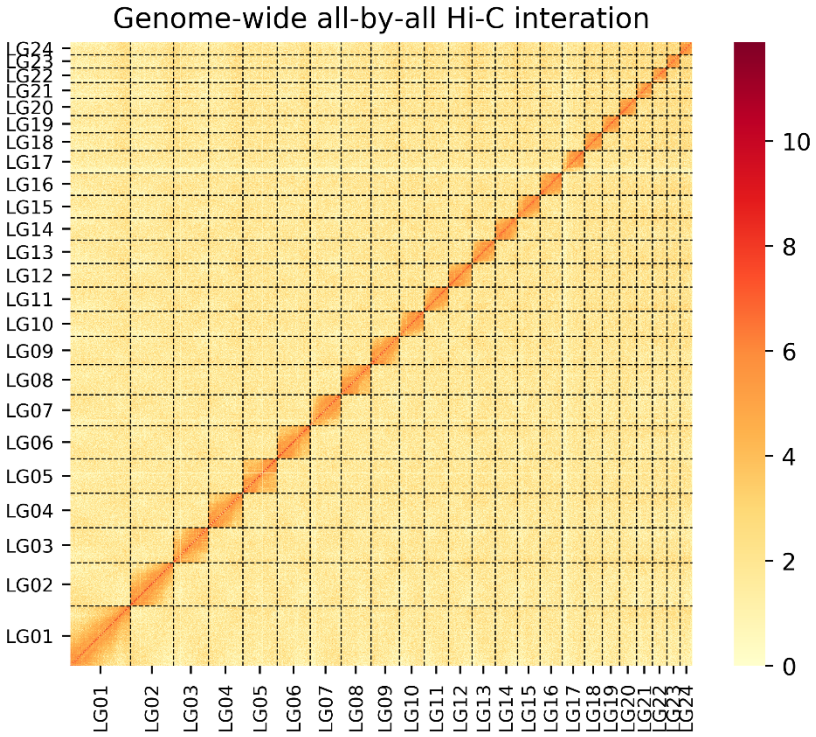

Supplementary Figure S1 Heatmap of Hi-C interaction signals

Intensity of intrachromosomal interactions is higher than that between chromosomes, indicating good assembly quality.

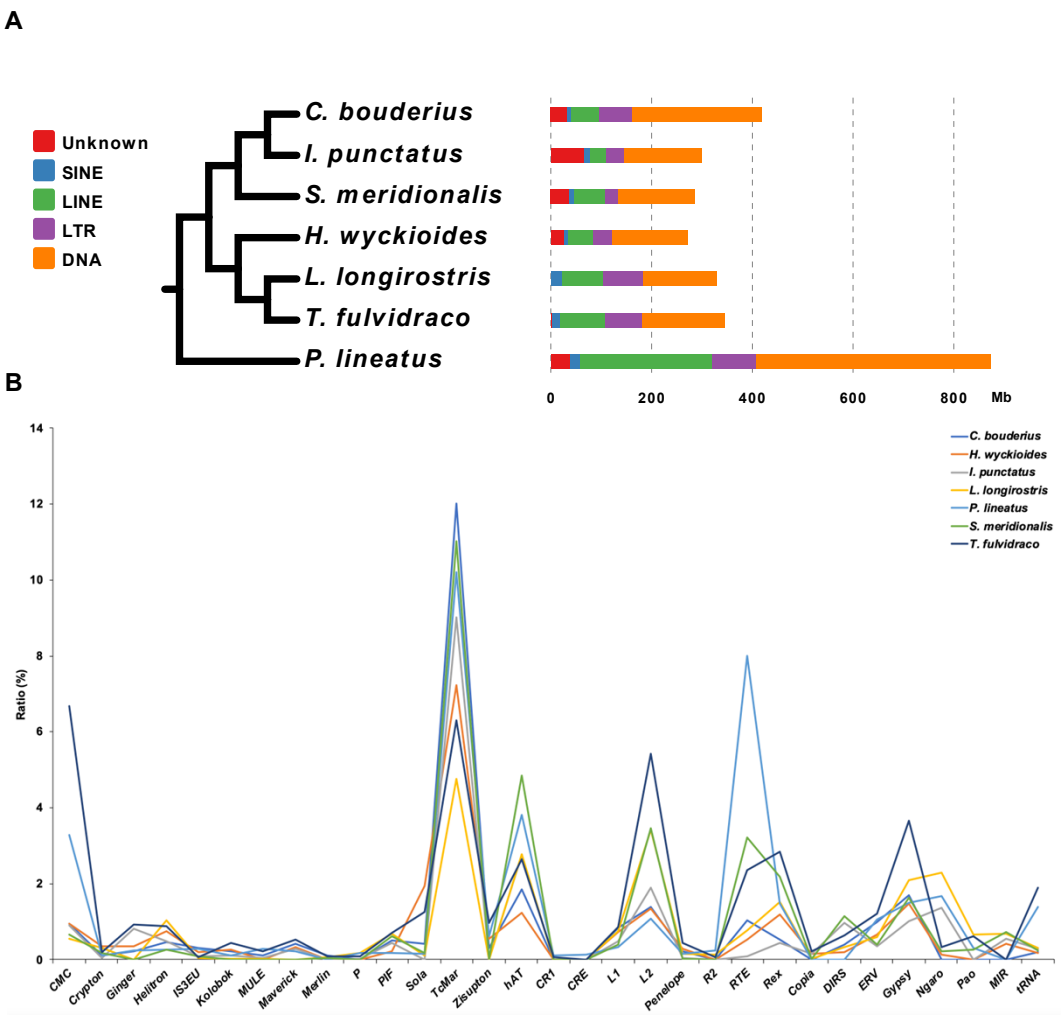

Supplementary Figure S2 TEs in *C. bouderius*, *H. wyckioides*, *I. punctatus*, *L. longirostris*, *P. lineatus*, *S. meridionalis*, and *T. fulvidraco*

A: Length of TEs of different types in three genomes. Different types of transposons are shown in different colors. B: Ratio of TEs of different types in three genomes. Different colored lines represent different species, TE superfamilies with concentrations greater than 0.1% in at least one selected species are shown.

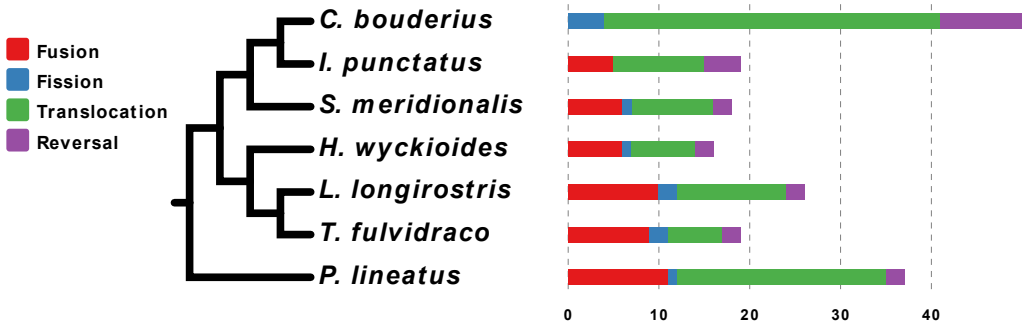

Supplementary Figure S3 Estimated number of chromosomal rearrangements from last common ancestor (LCA) of Siluriformes to each species

Different colors represent different types of rearrangement.

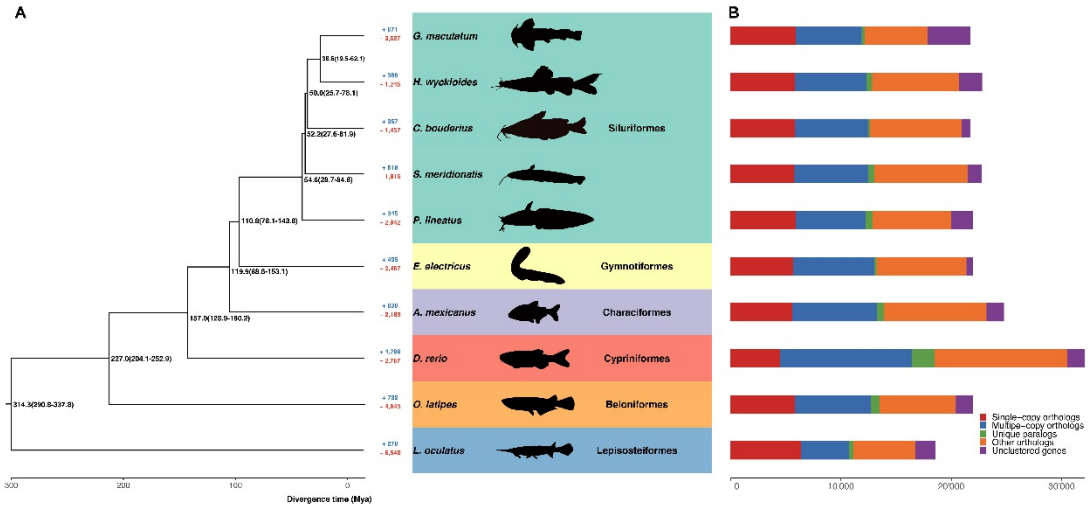

Supplementary Figure S4 Evolutionary genomics of *P. lineatus*

A: Phylogenetic relationships among selected Siluriformes. Numbers on nodes represent time of species differentiation. Numbers at end of branches represent number of expanded gene families and contracted gene families of corresponding species. B: Statistics of orthologous genes between selected Siluriformes.

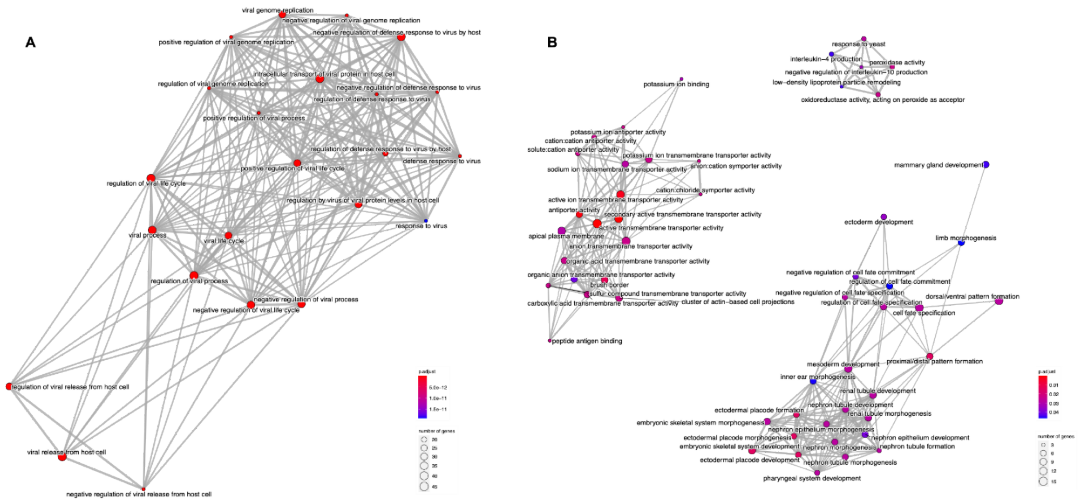

Supplementary Figure S5 GO enrichment results

A: GO enrichment results of *P. lineatus* expanded gene families associated with viral response. B: GO enrichment results of DO tissue-specific expressed genes.

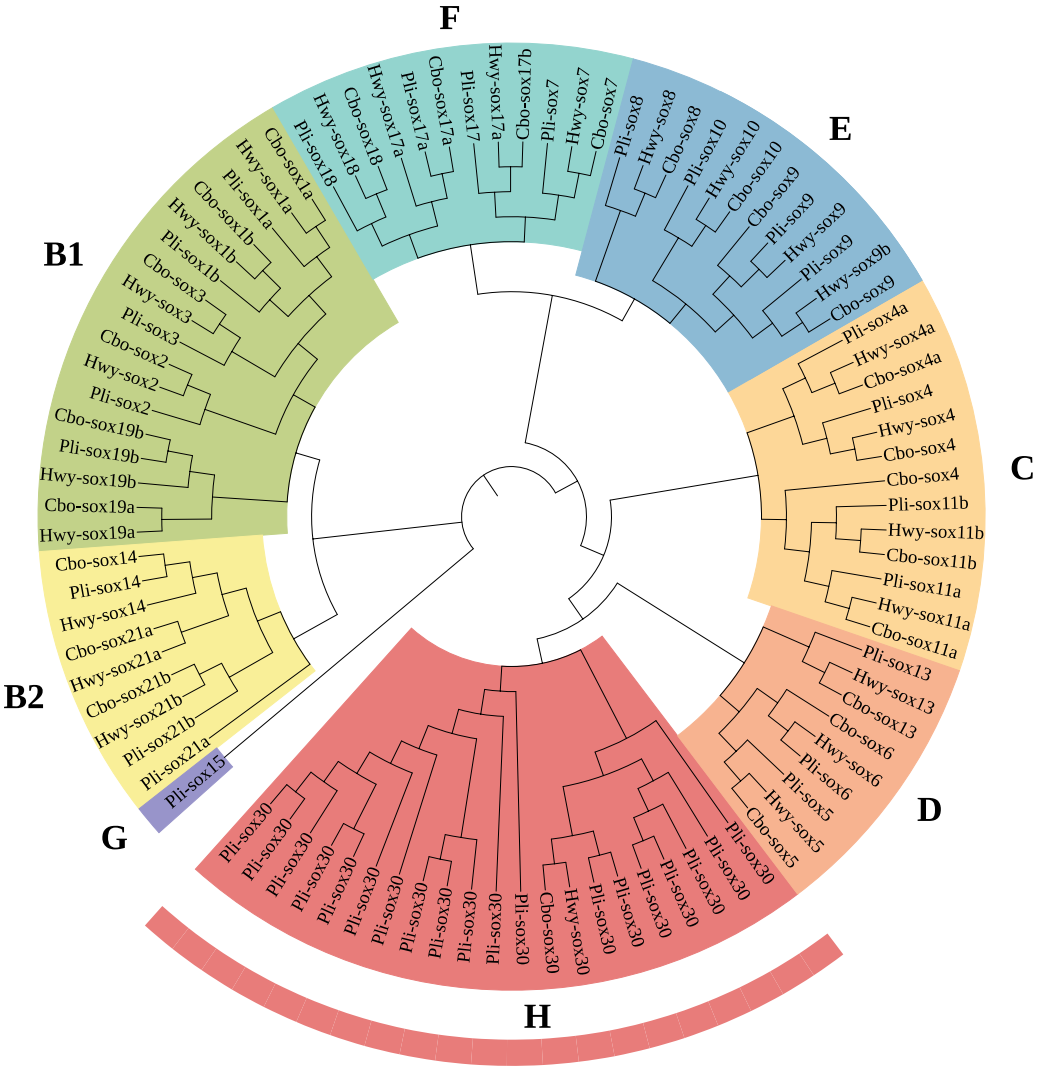
F
E
C
D
H
G
B2
B1
Pli-sox8
Hwy-sox8
Cbo-sox8
Pli-sox10
Hwy-sox10
Cbo-sox10
Cbo-sox9
Pli-sox9
Hwy-sox9
Pli-sox9
Hwy-sox9b
Cbo-sox9
Pli-sox4a
Hwy-sox4a
Cbo-sox4a
Pli-sox4
Hwy-sox4
Cbo-sox4
Cbo-sox4
Pli-sox11b
Hwy-sox11b
Cbo-sox11b
Pli-sox11a
Hwy-sox11a
Cbo-sox11a
Pli-sox13
Hwy-sox13
Cbo-sox13
Cbo-sox6
Hwy-sox6
Pli-sox6
Pli-sox5
Hwy-sox5
Cbo-sox5
Pli-sox30
Pli-sox30
Pli-sox30
Pli-sox30
Pli-sox30
Pli-sox30
Pli-sox30
Pli-sox30
Pli-sox30
Pli-sox30
Pli-sox30
Pli-sox30
Pli-sox30
Pli-sox30
Hwy-sox30
Cbo-sox30
Pli-sox30
Pli-sox30
Pli-sox30
Pli-sox30
Pli-sox30
Pli-sox30
Pli-sox30
Pli-sox30
Pli-sox30
Pli-sox30
Pli-sox30
Pli-sox30
Pli

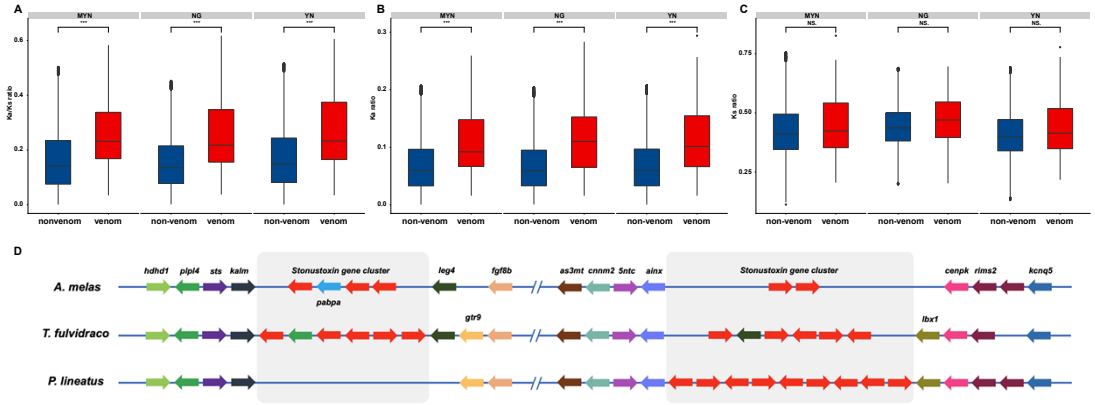

Supplementary Figure S7 Box plots comparing distributions of Ka/Ks (A), Ka (B), and Ks (V) values of venom-like and non-venom genes in *P. lineatus* and *A. melas*. Venom represents venom-like gene pairs of *P. lineatus* and *A. melas* obtained by homologous alignment, while non-venom represents gene pairs of *P. lineatus* and *A. melas*, excluding venom-like gene pairs. (D) Tandem duplication of *stonustoxin* genes in *P. lineatus*; *A. melas*, *T. fulvidraco*, and *P. lineatus* represent *stonustoxin* and adjacent genes. Synteny of genes around *stonustoxin* genes is illustrated by different colors. Gray areas connect *stonustoxin* gene clusters across species.

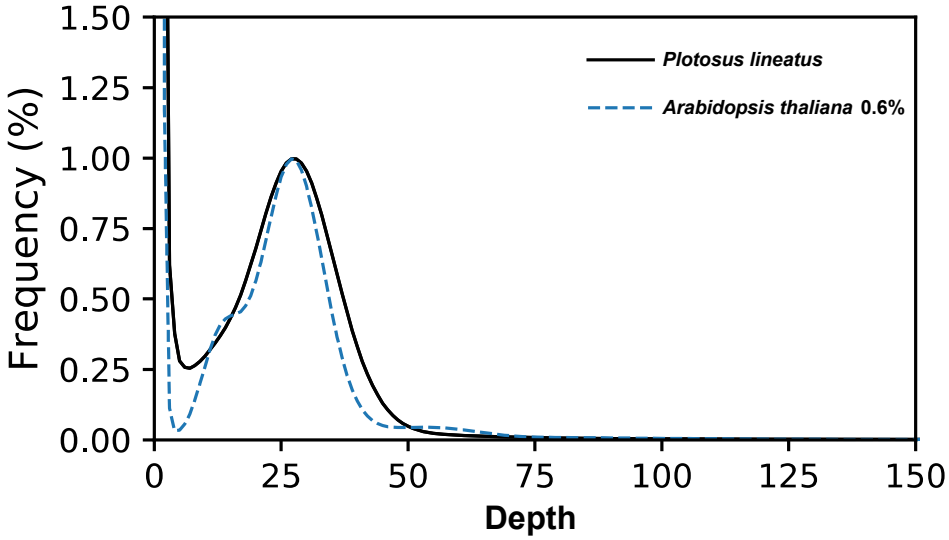

Supplementary Figure S8 Frequency distribution of 35 mer graph analysis used to estimate size of *Plotosus lineatus* (black line) and *K-mer* curve fitting was used to estimate heterozygosity of *P. lineatus* (blue dotted line).

Supplementary Tables

Supplementary Table S1 Summary of final *P. lineatus* genome assembly

Assembly index	Value
Contig number	111
N50	36,883,020
N90	8,315,259
Longest contig length	91,334,651
Total	1,333,853,200

Supplementary Table S2 Summary of 24 pseudochromosomes in *P. lineatus* genome

Linkage groups	Length	Contig number
LG01	128,135,270	6
LG02	92,328,563	4
LG03	74,941,363	5
LG04	73,950,024	3
LG05	73,028,679	6
LG06	71,125,833	1
LG07	65,578,422	6
LG08	64,393,414	3
LG09	60,384,906	4
LG10	53,384,567	9
LG11	52,100,826	2
LG12	50,546,027	1
LG13	49,018,779	8
LG14	48,077,731	2
LG15	47,936,828	1
LG16	47,594,762	6
LG17	46,357,040	23
LG18	38,807,430	2
LG19	36,773,966	2
LG20	36,115,174	2
LG21	33,994,089	2
LG22	31,023,330	4
LG23	28,471,796	2
LG24	26,424,324	1
Total	1,330,493,143	105

Supplementary Table S3 BUSCO assessment of *P. lineatus* genome assembly

Type	Number	Percent(%)
Complete BUSCOs (C)	932	97.69
Complete and single-copy BUSCOs (S)	909	95.28
Complete and duplicated BUSCOs (D)	23	2.41
Fragmented BUSCOs (F)	11	1.15
Missing BUSCOs (M)	11	1.15
Total	954	100

Supplementary Table S4 BUSCO assessment of *P. lineatus* gene structure annotation

Type	Number	Percent(%)
Complete BUSCOs (C)	4,254	92.80
Complete and single-copy BUSCOs (S)	4,026	87.83
Complete and duplicated BUSCOs (D)	228	4.97
Fragmented BUSCOs (F)	134	2.92
Missing BUSCOs (M)	196	4.28
Total	4,584	100.00

Supplementary Table S5 Statistics of gene functional annotation

Type	Number	Percent(%)
Complete BUSCOs (C)	4,254	92.80
Complete and single-copy BUSCOs (S)	4,026	87.83
Complete and duplicated BUSCOs (D)	228	4.97
Fragmented BUSCOs (F)	134	2.92
Missing BUSCOs (M)	196	4.28
Total	4,584	100.00

Supplementary Table S6 Statistics of repeat element annotation

Class	Order	Super family	Number of elements	Length of sequence (bp)	Percentage of sequence (%)
Class I			1,590,662	369,377,499	27.69
	LINE		722,123	260,706,981	19.55
		L2	113,009	14,543,261	1.09
		Unknown	237,150	101,196,416	7.59
		L1	28,766	2,235,818	0.17
		RTE-BovB	183,239	106,665,935	8.00
		Rex-Babar	50,034	19,618,757	1.47
		Penelope	33,866	2,082,438	0.16
		L1-Tx1	14,218	2,303,091	0.17
		CRE	8,690	1,841,167	0.14
		CR1	11,175	1,517,045	0.11
		R2-Hero	5,603	3,190,948	0.24
		Other	36,373	5,512,105	0.41
	LTR		681,180	87,083,630	6.53
		ERV1	111,638	11,959,426	0.90
		Gypsy	128,823	19,870,449	1.49
		Unknown	151,073	25,408,540	1.90
		Ngaro	217,173	22,246,332	1.67
		Pao	23,614	4,145,511	0.31
		ERVK	34,057	1,979,040	0.15
		Other	14,802	1,474,332	0.11
	SINE		187,359	21,586,888	1.62
		tRNA-Core-RTE	39,169	6,576,533	0.49

		tRNA-V-RTE	26,022	3,512,466	0.26
		Unknown	23,302	1,920,394	0.14
		tRNA-V	78,449	8,438,436	0.63
		Other	20,417	1,139,059	0.09
Class II			3,398,873	465,801,625	34.92
	DNA		3,000,878	380,196,452	28.50
		Zisupton	96,382	8,173,467	0.61
		hAT-Tip100	77,208	6,093,231	0.46
		CMC-EnSpm	387,936	43,703,814	3.28
		TcMar-Tigger	480,738	80,098,091	6.00
		Ginger	54,158	3,314,830	0.25
		Unknown	669,125	98,565,048	7.39
		hAT-Ac	168,534	21,372,343	1.60
		PIF-Harbinger	48,904	2,336,425	0.18
		Kolobok-T2	34,856	1,645,200	0.12
		Maverick	68,086	2,843,623	0.21
		Crypton-V	35,204	1,391,936	0.10
		hAT-Charlie	124,832	23,440,649	1.76
		TcMar-Tc1	240,666	56,024,697	4.20
		P	42,462	2,395,966	0.18
		MULE-MuDR	51,040	3,904,970	0.29
		Sola-1	35,084	2,076,380	0.16
		IS3EU	39,570	3,796,079	0.28
		Other	346,093	19,019,703	1.43
	RC		73,648	3,553,055	0.27
		Helitron	73,648	3,553,055	0.27
	MITE		324,347	82,052,118	6.15

		Unknown	324,347	82,052,118	6.15
Total TEs			4,989,535	835,179,124	62.61
Tandem Repeats			205,231	9,285,759	0.70
	SSR		105,478	1,406,934	0.11
	Tandem repeat		99,753	7,878,825	0.59
Unknown			228,854	31,488,600	2.36
Simple repeats			22,217	3,402,620	0.26
Other			45,145	6,140,295	0.46
Low complexity			2,477	371,538	0.03
Total Repeats			5,493,459	885,867,936	66.41

Supplementary Table S7 Conserved regions and ancestral chromosomes of Siluriformes
Supplementary Table S8 Selected fusion and translocation sites (FTSs)
Supplementary Table S9 FTSs and corresponding chromosome transposon content (100 kb window)
Supplementary Table S10 Content of different transposon superfamilies in FTSs
Supplementary Table S11 Positively selected genes
Supplementary Table S12 Genes within expanded gene families
Supplementary Table S13 GO enrichment results of expanded gene families
Supplementary Table S14 KEGG enrichment results of expanded gene families
Supplementary Table S15 *Plotosus lineatus*, *Cranoglanis bouderius*, and *Hemibagrus wyckioides sox* gene family CDSs
Supplementary Table S16 Tissue-specific genes expressed in DO
Supplementary Table S17 GO enrichment analysis of DO tissue-specific expressed genes
Supplementary Table S18 KEGG enrichment analysis of DO tissue-specific expressed genes
Supplementary Table S19 Genes of transposons specifically expressed in DO tissue
Supplementary Table S20 *Plotosus lineatus* and *Ameiurus melas* annotated venom-related CDSs
Supplementary Table S21 KaKs calculator results of *P. lineatus* vs *A. melas*
Supplementary Table S22 Clean RNA-seq data of different tissues and mapping ratios

Supplementary Tables S7–S22 are listed as a separate excel file due to their large size.